PCP
PLANT & CELL PHYSIOLOGY

Excitation spillover from PSII to PSI measured in leaves at 77 K

Ichiro Terashima[1,2,3,*], Riichi Oguchi[3,4], Kimie Atsuzawa[5], Yasuko Kaneko[6] and Masaru Kono,[3,7]

[1]Institute of Molecular Biology, College of Life Sciences, National Chung Hsing University, 145 Xingda Rd., Sourth Dist., Taichung City 40227, Taiwan, [2]Institute of Sustainable Agro-ecosystem Services, Graduate School of Agricultural and Life Sciences, The University of Tokyo, 1-1-1 Midoricho, Nishitokyo 188-0002, Japan, [3]Department of Biological Sciences, School of Science, The University of Tokyo, 7-3-1 Hongo, Bunkyo-ku,Tokyo 113-0033, Japan, [4]Botanical Gardens, Osaka Metropolitan University, 2000 Kisaichi, Katano 576-0004, Japan, [5]Comprehensive Analysis Center for Science, Saitama University, 255 Shimo-Okubo, Sakura-ku, Saitama 338-8570, Japan, [6]Department of Natural Science, Faculty of Education, Saitama University, 255 Shimo-Okubo, Sakura-ku, Saitama 338-8570, Japan, [7]Astrobiology Center, National Institutes of Natural Sciences, 2-21-1 Osawa, Mitaka 181-8588, Japan

*Corresponding authors: Ichiro Terashima, E-mails, terashimaichiro@nchu.edu.tw, terashimaichiro6@gmail.com; Masaru Kono, E-mail, konom07@bs.s.u-tokyo.ac.jp

Received 18 April 2024; Accepted 6 January 2025

Regular Paper

Abstract

Heterogeneous distribution of PSI and PSII in thick grana in shade chloroplasts is argued to hinder spillover of chlorophyll excitations from PSII to PSI. To examine this dogma, we measured fluorescence induction at 77 K at 690 nm (PSII) and 760 nm (mostly PSI) in the leaf discs of *Spinacia oleracea*, *Cucumis sativus*, and shade-tolerant *Alocasia odora*, grown at high and low light, and quantified their spillover capacities. PSI fluorescence (*F*I) consists of the intrinsic PSI fluorescence (FI_α) and fluorescence caused by excitations spilt over from PSII (FI_β). When *F*I and *F*II parameters between State 1 and State 2, induced by weak far-red and blue light, were compared, PSII maximum fluorescence (FII_m) and FI_β were greater, and FI_α was smaller in State 1; thereby, the spillover ratio, $FI_\beta/(FI_\alpha + FI_\beta)$, was greater in State 1. When nonphotochemical quenching (NPQ) was induced, the spillover ratio decreased. Since analyses of F_v/F_mspectra tentatively suggested that ∼15% of F_m at 760 nm was from PSII, all data were corrected accordingly. Even after the correction, the spillover ratio in FI_m in State 1 ranged from 16% to 28%. The spillover ratios did not greatly differ between the species or growth light levels. Although extensive grana in low-light-grown plants would suggest that PSII and PSI are too separate for spillover, the ratios of nonappressed thylakoid membranes/total thylakoid membranes in *A. odora* chloroplasts were little affected by growth light and >40%. Spillover would occur efficiently in abundant nonappressed thylakoids and in the margins of appressed thylakoids.

Keywords: fluorescence induction; grana; state transitions; sun/shade chloroplasts

Introduction

Land plants are exposed to various light fluctuations. Sudden changes in the photon flux density (PFD) from low to high levels often cause photoinhibition in PSII and PSI (for a recent review, see Kono et al. 2024).

Plants have evolved several mechanisms to protect photosystems from photoinhibition. Leaf and chloroplast movements are effective (Kasahara et al. 2002, Pastenes et al. 2005), yet these are beyond the present scope. Nonphotochemical quenching (NPQ), by which chlorophyll excitations are dissipated as heat, has been studied most intensively. Hereafter, chlorophyll and chlorophyll excitation are abbreviated as Chl and E*, respectively (Symbols and abbreviations used in the present paper are listed at the end of the Materials and Methods section). Changes in the protein structure and the energy levels of the pigments in the PSII antenna systems due to protonation of PsbS protein and conversion of violaxanthin to zeaxanthin, via antheraxanthin, are responsible for NPQ (Bassi and Dall'Osto 2021). It has been proposed that, during NPQ induction, some light harvesting Chl protein complexes (LHCIIs) are clustered and functionally separated from the PSII core complexes and that E*s in such antenna clusters decay emitting heat (Ruban et al. 2012). At ordinary temperatures, it takes 5–10 min to induce NPQ mostly. Full conversion of violaxanthin to zeaxanthin takes some more time (Bassi and Dall'Osto 2021). Conversely, when the PFD level is lowered, NPQ is relaxed and the mechanism dissipates E*s as heat is turned off. The relaxation processes take several minutes as well.

For safe and efficient photosynthesis in the fluctuating light, NPQ should be induced and relaxed rapidly. Kromdijk et al. (2016) overexpressed three components involved in the induction and relaxation processes of NPQ, violaxanthin

Plant And Cell Physiology, 2025, 66(3), 358–373
doi:https://doi.org/10.1093/pcp/pcaf002
Advance Access publication on 7 January 2025

de-epoxidase, PsbS, and zeaxanthin epoxidase, in *Nicotiana tabacum* (tobacco). When gas exchanges of such leaves were assessed in the laboratory using red and blue light emitting diodes (LEDs) as actinic light, the NPQ relaxation processes were accelerated. In the field, where light fluctuates, these plants grew better than the wild type. Three lines of *Arabidopsis thaliana* overexpressing these three components showed faster NPQ induction and relaxation in the laboratory. However, neither of these lines grew better than the wild type in a natural light greenhouse. In an artificial fluctuating light in a growth chamber, these lines grew less than the wild type (Garcia-Molina and Leister 2020). Although the discrepancy of the results between their reports has not been resolved, the strong induction of NPQ might exert a negative effect on photosynthetic production *in A. thaliana* under their experimental conditions (Garcia-Molina and Leister 2020).

We recently found that far-red (FR) light accelerates NPQ relaxation in *A. thaliana* (Kono et al. 2020). It appears that the H^+/K^+ antiporter in thylakoid membranes (KEA3) is activated by FR light and accelerates NPQ relaxation (Kono et al., unpublished observation). The results of the field experiments by Kromdijk et al. (2016), therefore, would reflect this FR light effect on the rapid NPQ relaxation, because FR light is abundant in natural light.

State transitions realize balanced distribution of E*s between PSII and PSI by adjusting allocation of mobile LHCIIs between these photosystems. The LHCII movements from PSII to PSI and from PSI to PSII are caused by the phosphorylation and dephosphorylation of LHCIIs and the PSII core, and the responsible kinases have been identified. The state transitions were once thought to play roles in protecting PSII from photoinhibition in high light (Horton and Lee 1985, Anderson and Andersson 1988, Bellaflore et al. 2005). However, it has been revealed that these kinases are inactivated in high light *in vivo* (Rintamäki et al. 1997, Pursiheimo et al. 1998). Moreover, the mutant deficient in one of these kinases, *stn7*, grew well in continuous high light. Since *stn7* did not grow well in the fluctuating light, LHCII phosphorylation may play a role in acclimation to the fluctuating light (Grieco et al. 2012).

The spillover denotes transfer of E*s from PSII to PSI. Analyses of fluorescence induction at 77 K revealed that induction of PSI fluorescence occurred synchronously with that of PSII. Spillover occurs even in the absence of closed PSII. When PSII reaction centres close, more E*s are transferred to PSI. This mechanism was first described by Murata (1969). Soon after, theoretical analyses were made (Kitajima and Butler 1975a, b, Kitajima 1976, Strasser and Butler 1977a, b). Since the spillover prevents accumulation of E*s around the closed PSII reaction centres, the intersystem crossing of the excited Chls in the singlet state (^{S}Chl*s) to those in the triplet state (^{T}Chl*s) around or in the reaction centres is suppressed. Although the energy level of ^{T}Chl* is lower than that of ^{S}Chl*, its lifetime is longer than that of ^{S}Chl* by 3 orders of magnitude (Khorobrykh et al. 2020). Thus, once ^{T}Chl*s are formed, the chance of $^S O_2$ formation increases. Hence, the spillover alleviates PSII photoinhibition. E*s transferred from PSII to PSI oxidize P700 to $P700^+$, the key component for protection of PSI from photoinhibition (Miyake 2020). Therefore, the spillover protects not only PSII but also PSI from photoinhibition (Terashima et al. 2021, Kono et al. 2024).

The extent of NPQ is smaller in shade plant leaves than in sun plant leaves, due to the smaller pool size per leaf area of xanthophyll cycle carotenoids in shade leaves (Demmig-Adams and Adams 2006). Shade plants in the canopy understories are often exposed to sunflecks (Pearcy 1990, Pearcy and Way 2012) or sun patches (Smith and Berry 2013). To avoid photoinhibition due to such drastic changes in PFD, spillover would be more efficient than NPQ, because spillover occurs instantaneously, while induction of NPQ requires several minutes. Shade plants, therefore, might rely more on the spillover than sun plant leaves to avoid photoinhibition.

After the classical studies for spillover quantification (Kitajima and Butler 1975a, b, Kitajima 1976, Strasser and Butler 1977a, b), there had been few attempts to quantify spillover. Recently, researchers resumed to study spillovers in various organisms using time-resolved fluorescence spectroscopy (Chukhutsina et al. 2019). Megacomplexes have also been attracting attention, and the spillover is claimed to occur in the PSI–PSII megacomplexes, which include the PSI, PSII, and LHC complexes (Yokono et al. 2015, Ifuku 2023, Kim et al. 2023). If this is true, transfer of E*s would occur in the single membrane because the megacomplex exists in a single thylakoid membrane.

Thylakoid membranes are categorized into appressed and nonappressed membranes. The appressed membranes occur inside the grana in contact with other appressed membranes, while the nonappressed membranes directly face the stroma, forming the intergranal thylakoids or the grana surface membranes. In the thylakoid membranes, distributions of the major protein complexes are heterogeneous (Anderson and Andersson 1988). PSII complexes are mainly in the appressed membranes, while PSI complexes and H^+-ATPases are mainly in the nonappressed membranes. Since the PSII complexes in the appressed membranes are located distant from the PSI complexes in the nonappressed membranes, it would be unlikely for E*s to be transferred from PSII to PSI across the membranes. Yet, the transfer of E*s across the membranes was claimed to occur based on measurements of electrogenicity in thylakoid preparations (Trissl et al. 1987).

It is known that the chloroplast morphologies are different between sun and shade plants. Grana in shade plant chloroplasts are generally thicker and contain more thylakoids (Björkman 1981, Anderson 1986). Similar trends have been reported for sun and shade leaves of the same species (Björkman 1981, Anderson 1986) and even for the adaxial and abaxial parts in the same leaf (Skene 1974, Terashima et al. 1986). These morphological features imply that spillover would occur more easily in sun-type chloroplasts that have thinner grana. Chow et al. (1988) showed an electron micrograph of gigantic grana in a leaf of low-light-grown *Alocasia macrorrhiza*, a shade-tolerant Araceaenspecies. The number of thylakoids per granum exceeded 100. These impressive grana suggest that the spillover of E*s from PSII to PSI might be hampered.

In a recent paper, in which the spillover in *Pinus sylvestris* (Scots pine) leaves was detected by time-resolved fluorescence analysis, the authors concluded that the increase in the spillover was accompanied by the decrease in the number of thylakoids per granum or by thylakoid de-stacking (Bag et al. 2020). Yokono et al. (2019) surveyed the existence of the megacomplexes in various green plants and found that sun plants accumulate more PSI–PSII megacomplexes than shade plants. They found a tendency that PSI of sun plants had deeper traps (low-energy Chls) to receive excitation energy and showed PSI fluorescence maxima at wavelengths longer than 730 nm. Unfortunately, typical shade-tolerant plants were not included in their plant materials (Table 1 of Yokono et al. 2019). Based on the spectroscopic evidence of the deep-trap Chl *a* in leaves of a shade-tolerant *Alocasia odora*, we proposed that the shade-tolerant plants also have PSI–PSII megacomplexes and, due to the deep-trap Chl *a*, spillover of the excitation energy from PSII to PSI would contribute to formation of $P700^+$ in high light (Terashima et al. 2021, Kono et al. 2024).

In the present study, we grew sun species, such as *Spinacia oleracea* (spinach) and *Cucumis sativus* (cucumber), and a shade-tolerant species, *A. odora* at different light levels. *A. odora* was used, because we are interested in the mechanisms for photoinhibition avoidance in this species (Terashima et al. 2021). *Hordeum vulgare* (barley), a wild type and a Chl *b*-less mutant lacking most LHCIIs, were also grown. We measured the induction of PSII fluorescence at 690 nm and that of mostly PSI fluorescence at 760 nm in leaf discs of these plants frozen at 77 K. We divided PSI fluorescence into the fractions corresponding to the PSI fluorescence caused by E*s spilt over from PSII and the intrinsic PSI fluorescence. The spillover ratios were compared among the species and between the growth light levels. A substantial spillover was detected in the leaves of low-light-grown *A. odora*. Moreover, the spillover was not necessarily greater in high-light-grown plants. The barley *b*-less mutant also showed considerable spillover. Effects of NPQ induction and $P700^+$ formation on the intrinsic PSI fluorescence were also investigated using low-light-grown *A. odora*. Since the differences in ultrastructure between the chloroplasts from high- and low-light-grown *A. macrorrhiza* (Chow et al. 1988) were intriguing, we quantitatively analysed the thylakoid ultrastructure of *A. odora* to elucidate the inter-relationship between the ratio of nonappressed thylakoid membranes and total thylakoid membranes, thylakoid stacking, and the spillover. During the present study, however, we found a substantial leftover PSII fluorescence at 760 nm. We, therefore, tried to estimate the leftover PSII fluorescence and its effect on the spillover. The effect of excitation of PSI Chls by PSII fluorescence was also considered.

Results

Fluorescence induction

The leaf disc on wet paper was irradiated with LEDs peaked at 720 nm (PSI light) or 470 nm (PSII light) at a PFD of 10 or 5 μmol m^{-2} s^{-1} for at least 30 min to allow transitions to State 1 or State 2. The disc was then placed in an aluminium cup, kept in the dark for 1.5–2 min, and frozen to 77 K. Induction of fluorescence excited by blue light at 460 nm at 50 μmol m^{-2} s^{-1} was measured either at 690 nm or 760 nm for PSII fluorescence (*F*690) or mostly PSI fluorescence (*F*760) at 1-ms time intervals for 30 s. Both *F*690 and *F*760 showed typical inductions (Fig. 1a). It took about 5 s to attain F_m levels. When *F*760(*t*) was plotted against *F*690(*t*), a linear line was obtained (Fig. 1b). See Table 1 for the plant materials. For the measurement system, see Supplementary Figs. S1 and S2.

For simplicity, let us first assume that fluorescence signals detected at 690 and 760 nm were exclusively from PSII and PSI and that the induction of *F*760 is attributed to the spillover of E*s from PSII (Kitajima and Butler 1975, Butler and Kitajima 1975, Kitajima 1976, Strasser and Butler 1977a, b). *F*760(*t*) is, then, expressed as follows:

$$F760\,(t) = F_\alpha 760 + \sigma F690\,(t)\,, \qquad (1)$$

where σ is the spillover coefficient, which is equal to the ratio of variable fluorescence at 760 nm to that at 690 nm, F_v760/F_v690. When F_m was attained,

$$F_m 760 = F_\alpha 760 + \sigma F_m 690 = F_\alpha 760 + F_\beta 760. \qquad (2)$$

Then, the proportion of the spillover in PSI fluorescence was calculated as $F_\beta 760/F_m 760$ or $F_\beta 760/(F_\alpha 760 + F_\beta 760)$. For a diagrammatical explanation of the relationships between *F*760 and *F*690, see Supplementary Fig. S3A.

The effects of growth light and state transitions on F_v690/F_m690 and F_v760/F_m760 are shown in Table 1. Except for one case of the high light-grown (HL) *A. odora*, the differences in F_v690/F_m690 depending on the states were not statistically significant, while F_v760/F_m760 was greater in State 1. The effects on F_m690, $F_\alpha760$, and F_m760 are shown in Table S1. In these calculations, we assumed that there was no leftover PSII fluorescence (*F*II) at 760 nm. When the data for the same leaf materials were compared, F_m690 was always greater in State 1, consistent with the view of LHCII movement from PSI to PSII in State 1 light. Inversely, PSI intrinsic fluorescence level ($F_\alpha760$) was greater in State 2. F_m760 is the sum of $F_\alpha760$ and that is caused by the spillover from PSII, $F_\beta760$. $F_\alpha760$ was greater in State 2, while $F_\beta760$ would be greater in State 1, which resulted in the situation where there was no consistent effect of the state on F_m760. These trends are relevant even when the leftover *F*II at 760 nm was considered (Table 3, Fig. 4, and Table S2).

We also examined the induction time course (Table S1). Mobile LHCIIs would move from PSII to PSI in State 2 light and *vice versa* in State 1 light. Then, faster induction of *F*690 was expected to occur in State 1, because antenna size per PSII reaction centre would increase in State 1. When HL and low light-grown (LL) leaves were compared, Chl *a*/*b* was lower in LL leaves (Table 1), indicating that LHCIIs were more abundant in LL leaves. Thus, the induction would be faster in LL leaves. Both these trends were observed (Table S1).

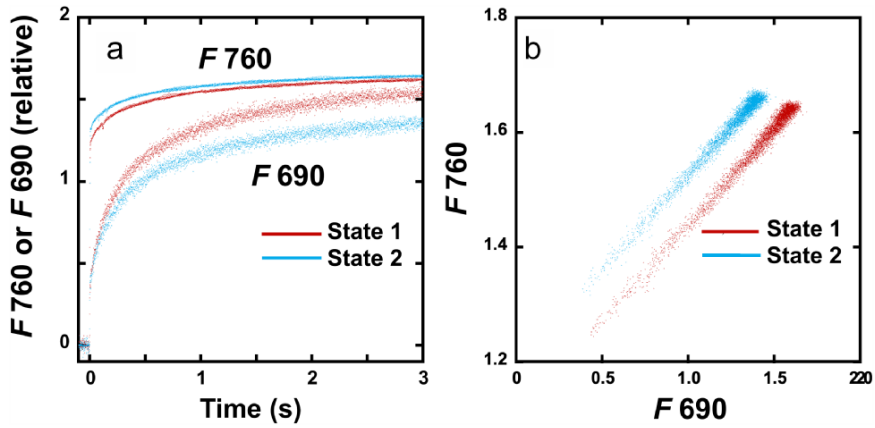

Figure 1. Induction curves of *F*690 and *F*760 and the relationships between *F*690 and *F*760 in LL *A. odora*. (a) PSII fluorescence (*F*690) and mostly PSI fluorescence (*F*760) induction measured at 690 and 760 nm in leaf discs at 77 K of LL *A. odora*. Leaf discs were illuminated with PSI light at 720 nm inducing State 1 or PSII light at 470 nm inducing State 2, at the PFD of 5 μmol m^{-2} s^{-1}, for at least 30 min, kept in the dark for 1.5–2 min and frozen in liquid N_2. Fluorescence induction excited by the measuring/actinic light from a 460-nm LED pulse-modulated at 100 kHz was recorded. The PPFD level of the measuring/actinic light at the leaf disc was 50 μmol m^{-2} s^{-1}. (b) *F*760 plotted against *F*690.

Table 1. Chl content and Chl *a*/*b* of the samples and the effects of state transitions on F_v690/F_m690 (*RV*690) and F_v760/F_m760 (*RV*760)

	Growth light (μmol m^{-2} s^{-1})	Chl (mmol m^{-2})	Chl *a*/*b*	State	*RV*690	*RV*760
Cucumis sativus	400	0.26 ± 0.024	5.08 ± 0.141**	1	0.850 ± 0.018	0.319 ± 0.008***
				2	0.836 ± 0.019	0.290 ± 0.006
	100	0.25 ± 0.028	4.06 ± 0.080	1	0.824 ± 0.005	0.316 ± 0.009**
				2	0.823 ± 0.014	0.277 ± 0.014
Spinacia oleracea	400	0.62 ± 0.048**	3.86 ± 0.073**	1	0.781 ± 0.033	0.299 ± 0.029**
				2	0.794 ± 0.019	0.238± 0.012
	100	0.49 ± 0.034	3.59 ± 0.105	1	0.777 ± 0.042	0.297 ± 0.016**
				2	0.793 ± 0.019	0.244 ± 0.017
Alocasia odora	100			1	0.851 ± 0.006**	0.246 ± 0.018**
		0.63 ± 0.024**	3.96 ± 0.025**	2	0.810 ± 0.014	0.202 ± 0.009
	10	0.54 ± 0.035	3.52 ± 0.041	1	0.774 ± 0.015	0.265 ± 0.012**
				2	0.755 ± 0.027	0.224 ± 0.017
Hordeum vulgare wild type	400	0.38 ± 0.068**	3.75 ± 0.194	1	0.822 ± 0.028	0.274 ± 0.025*
				2	0.797 ± 0.021	0.232 ± 0.009
H. vulgare Chl *b* less	400	0.18 ± 0.027	»	1	0.731 ± 0.059	0.238 ± 0.010
				2	0.694 ± 0.017	0.226 ± 0.007

Each of the data are shown as the mean ± SD ($n = 4$). Chl *a*/*b* ratio in the Chl *b*-less barley was not determined and was noted by ».
*, **, and *** denote $P < .05$, .01, and .001, respectively, according to *t*-test.

Effects of the leftover PSII fluorescence (*FII*) at 760 nm

Hereafter, we use *F*I and *F*II to denote PSI and PSII fluorescence. Fluorescence emission spectra of the PSI particles at 77 K (Lamb et al. 2018 and the references therein) indicate that there may be no PSI fluorescence (*F*I) at 690 nm. On the other hand, the PSII particles show some *F*II at 760 nm.

To assess the leftover *F*II at longer wavelengths beyond the *F*I peak, we measured fluorescence at wavelengths ranging from 690 to 780 nm. If there is *F*II at long wavelengths, F_v/F_m will increase with the decrease in PSI fluorescence, because FII_v/FII_m is greater than FI_v/FI_m. We also measured fluorescence emission spectra of F_m in the leaf discs with a photodiode array spectrophotometer. In these measurements, the leaves of *C. sativus*, *S. oleracea*, and *A. odora* were used. The leaf discs were frozen after illumination of the State 1 light, because *F*II and possible leftover *F*II would be enhanced in State 1. For simplicity, we often express the variable fluorescence to maximum fluorescence ratio as *RV*, instead of F_v/F_m.

Figure 2a shows emission spectra of F_m in State 1. *Cucumis sativus* and *A. odora* showed peaks at 740 nm, while the peak of *S. oleracea* occurred at 737 nm. The spectra for *RV* in State 1 are shown in Fig. 2b. At 690 nm, *RV* in *S. oleracea* was low, indicating chronic photoinhibition. These materials were different from those used for the data shown in Table 1 (see the Materials and Methods section). In all these samples, *RV* decreased toward 750 nm and then *RV* increased, indicating some leftover *F*II at wavelengths > 750 nm. For a diagrammatical explanation of effects of the leftover *F*II on *F*I induction, see Supplementary Fig. S3B.

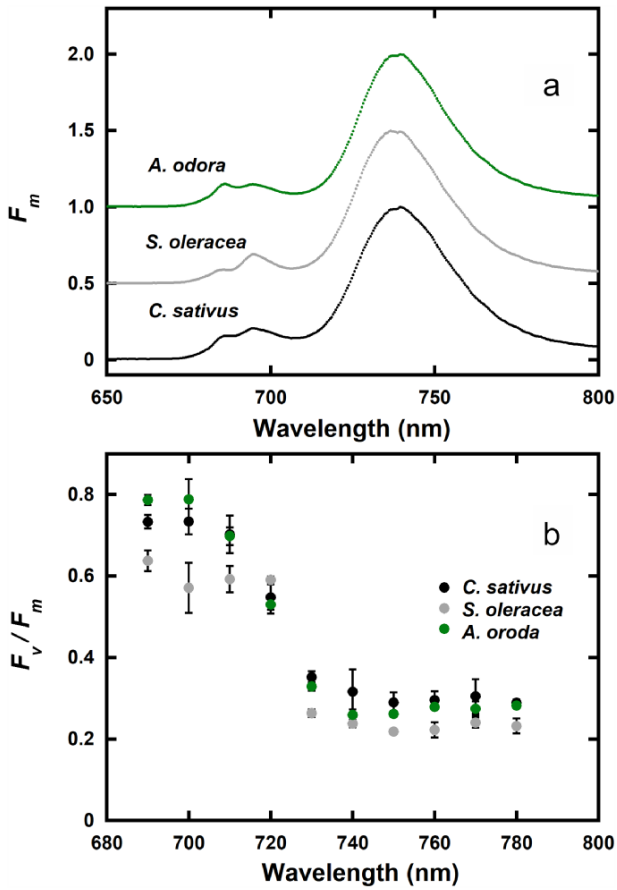

Figure 2. F_m spectra (a) and F_v/F_m spectra (b) for the wavelength range from 690 to 780 nm in *C. sativus*, *S. oleracea*, and *A. odora* leaf discs. (a) Emission spectra of F_m, excited by blue light from an LED peaked at 450 nm, were measured using a photodiode array spectrophotometer (C10083CAH, Hamamatsu Photonics, Japan). The F_m spectra were not corrected for the sensitivity of the photomultiplier. For each species, only average values of three measurements are shown. (b) F_v/F_m values in the leaf discs were measured using the band pass filters (Asahi Spectra). The mean ± standard deviation are shown ($n = 3$). For both (a) and (b), the leaf discs were treated in State 1 light at 720 nm at 10 μmol m^{-2} s^{-1} at least for 30 min, kept in dim light or in the dark for 1.5–2 min, and frozen at 77 K.

Since we used leaf discs, reabsorption of fluorescence by Chl distorted the spectral shape at short wavelengths. However, the fluorescence levels at the long wavelengths may be used for quantitative analyses. Because PSII fluorescence data of the PSII particles, except for those with obvious contamination of PSI components, often show monotonous decreases toward the long wavelengths (Lamb et al. 2018 and the references therein), we first assumed that the leftover FII_m can be expressed as a linear function of wavelength (λ) for a range (730 nm $\leq \lambda \leq$ 780 nm). Then, FI_m at the wavelength λ nm, $FI_m\lambda$, was expressed as $F_m\lambda - FII_m\lambda$. F_v/F_m (*RV*) at λ, $RV\lambda$, was also expressed with $F_m\lambda$, $FII_m\lambda$, *RV*II, and *RV*I (for details, see the Supplementary Text 1). Assuming that *RV*II was equal to F_v/F_m at 690 nm, *FV*690, we obtained a set of three independent variables, the slope and the intercept of the linear function expressing $FII_m\lambda$, and *RV*I, which minimized the residual sum of squares of the differences (RSSs) between the model and the measured *RV* values at 730, 740, 750, 760, 770, and 780 nm. The *RV*I values and the ratios of FII_m to total F_m at 760 nm, thus obtained, are shown in Table 2. At 760 nm, FII_m was estimated to be 8% of F_m for *S. oleracea*, 10% for *C. sativus*, and 16% for *A. odora*. For the fitting of the data, see Supplementary Fig. S4. Although changes of in F_v/F_m with wavelength were not simple, the modelled values overlap well with the measured values.

Second, to consider the effects of PSII spectra bearing vibronic shoulders or peaks at ∼750 nm, we digitized four such spectra (Van Dorssen et al. 1987, Ruban and Johnson 2009, Karlický et al. 2010) of the PSII particles (Supplementary Fig. S5A). The average of these four fluorescence spectra was well fitted by a cubic function, and as above, we obtained *RV*I and the constant for expressing $FII_m\lambda$ that minimized RSS (Table 2). However, the *RV*I value was greater than *RV*760 in all the species, and the fitting was poor (Supplementary Fig. S5B). Among these four curves, one curve was fitted by a quadratic curve well. Using this curve, we also obtained *RV*I and a constant for $FII_m\lambda$ that minimize RSS (Table 2). At 760 nm, FII_m was estimated to be 13% for *S. oleracea*, 14% for *C. sativus*, and 18% for *A. odora*. Fitting was better than those by the linear function (Supplementary Fig. S5B). These results indicate that the compound changes in the F_v/F_m values would be attributed to a long tailing of FII_m and the substantial level of FII_m around the *FI* peak. Given that fitting by the linear functions (Supplementary Fig. S4) and by the quadratic function (Supplementary Fig. S5B) was good, we may tentatively assume that the leftover level of *FII* fluorescence at 760 nm would be 10%–20%.

Spillover ratios are shown in Fig. 3 and Table 3. The data in Fig. 3 were calculated assuming no *FII* leftover at 760 nm. For the spillover ratios assuming 0%, 5%, 10%, 15%, and 20% FII_m/F_m at 760 nm, see Table 3. As expected from *RV*760 data in Table 1, spillover ratios were consistently greater in State 1 light. When HL and LL discs were compared, the levels were comparable in *S. oleracea*. But in *C. sativus* and *A. odora*, the values were significantly greater in LL discs. The leaves of shade-tolerant *A. odora* showed the value of >0.3 in State 1. The *b*-less barley mutant also showed considerable spillover above 0.3. It is noteworthy that there were no effects of the state light on fluorescence data in the *b*-less barley, in which LHCIIs are mostly absent.

Effects of *FII* leftover at 760 nm on the spillover ratios in PSI fluorescence are shown in Table 3. For a given leftover ratio, if we assume that *RV*II is identical to *RV*690, *RV*I and the spillover ratio (FI_β/FI_m) can be calculated. Note that, for FI_β to be positive, $RV760/RV690 > \gamma$. It should also be noted that FI_α is constant irrespective of γ (see equations in the note of Table 3). Since *RV*750 was actually smaller than *RV*760 (Fig. 2), the maximum γ is further smaller: $RV750/RV690 > \gamma$. When the leftover was 15%, spillover ratios in State 1 ranged from 16% to 28%. We

Table 2. FI_v/FI_m (RVI) giving the least residual sum of squares of the differences and the leftover ratio of FII_m760/F_m760 at 760 nm

		$RVII$	$RV760$	RVI	$\frac{RVI}{RV760}$	$\frac{FII_m760}{F_m760}$	RVI
Linear	*Cucumis sativus*	0.733	0.290	0.241	0.831	**0.100**	*
	Spinacia oleracea	0.637	0.222	0.185	0.833	**0.082**	*
	Alocasia odora	0.787	0.279	0.182	0.652	**0.160**	*
Vibronic (cubic)	*C. sativus*			0.318	>1		***
	S. oleracea			0.237	>1		***
	A. odora			0.282	>1		***
Quadratic	*C. sativus*			0.218	0.752	**0.140**	**
	S. oleracea			0.162	0.730	**0.126**	**
	A. odora			0.171	0.613	**0.175**	**

The FII_m760/F_m760 ratios are highlighted in bold to emphasize their importance. The significance level of RVI denotes that each of the RVI values is significantly different from 0.
*, **, or *** denote $P < .05$, .01, and .001, respectively.

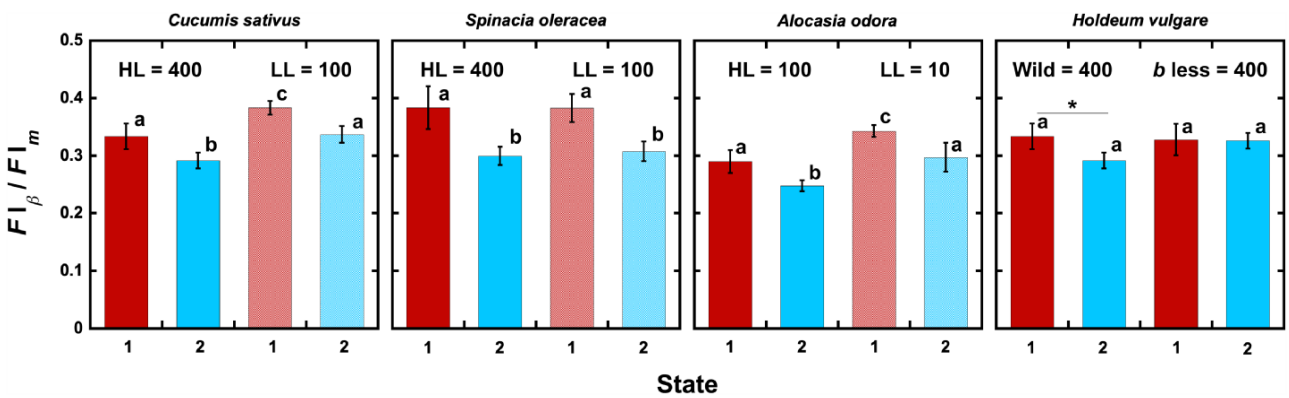

Figure 3. Spillover ratio (FI_β/FI_m) in leaf discs in State 1 and State 2. 1 and 2 on the abscissa denote State 1 and State 2, induced by PSI and PSII light at 10 μmol m^{-2} s^{-1} at least for 30 min. For LL *A. odora*, PSI or PSII light was at 5 μmol m^{-2} s^{-1}. HL and LL denote high and low growth light. 400, 100, and 10 denote growth PPFD levels in μmol m^{-2} s^{-1}. The mean ± standard deviation are shown ($n = 4$). Different alphabets denote statistically significant differences ($P < .05$) by ANOVA (Tukey–Kramer test). For HL and LL *H. vulgare*, *t*-test was used (* denotes $P < .05$). For the data in this figure, no leftover FII_m at 760 nm was assumed. For the effects of the FII leftover, see Table 3.

did not examine leftovers of FII in the wild type or the Chl *b*-less mutant of *H. vulgare*.

Effects of NPQ

Effects of NPQ formation on spillover were examined in the leaf discs from an LL *A. odora* leaf (Fig. 4 and Table S2). After the induction of NPQ by a white light at 700 μmol m^{-2} s^{-1} for 270 s at a room temperature of ca. 23°C, NPQ values, $(FII_m - FII_m')/FII_m'$, were measured at 23°C. Then, weak PSI light peaked at 720 nm was given for 10 s to oxidize the acceptor side of PSII, and the leaf disc was frozen.

Compared with sun plants, NPQ is modest in shade-tolerant plants mainly due to the lower contents of xanthophyll cycle carotenoids per leaf area (Demmig-Adams and Adams III 2006). Although LL *A. odora* was used and the actinic light was moderate, NPQ levels after the NPQ induction more than 1.2 were obtained. The differences in NPQ between the samples for $RV760$ (1.22 ± 0.119, mean ± standard deviation, $n = 4$) and for $RV690$ measurements (1.35 ± 0.090, $n = 4$) were not statistically significant ($P = 0.194$, *t*-test). The data in Fig. 4, which were calculated assuming 0% FII_m leftover at 760 nm, show smaller $F_\beta760$ and $F_\beta760/F_m760$ in the NPQ-induced leaf discs, indicating that the spillover of E*s from PSII to PSI decreased after the NPQ induction. $F_\beta760/F_m760$ in the dark-treated control was 0.3, which resembled the value in State 2 light in LL *A. odora* (Fig. 3), as Weis (1985) pointed out for *S. oleracea*. It is also noteworthy that $F_\alpha760$ was unaffected by NPQ. The effects of FII leftover at 760 nm on these data are shown in Table S2. The absolute value of the spillover ratio decreased with the increase in the leftover FII. It is noteworthy that, due to our assumptions, FI_α was constant irrespective of the leftover ratios and NPQ induction (see the equations in the note of Table 3).

Effects of $P700^+$ on PSI intrinsic fluorescence

To detect PSI intrinsic fluorescence, we used a pulse-modulated measuring/actinic beam that was peaked at 700 nm and at the PFD level of 0.07 μmol m^{-2} s^{-1}. Changes in the intrinsic PSI fluorescence are shown in Fig. 5. After 15 s from the onset of recording at 4-ms intervals, the measuring/actinic light was on. First, the noise reduction circuit was not used to examine whether there was an induction in the PSI intrinsic fluorescence. Even though the measuring/actinic light was very weak, no induction

Table 3. Effects of 0%, 5%, 10%, 15%, and 20% FII_m/F_m at 760 nm on FI_v/FI_m (*RVI*) and spillover ratio (FI_β/FI_m)

					RVI					Spillover ratio				
	Growth light (μmol m^{-2} s^{-1})	State	*RV*690	*RV*760	0%	5%	10%	15%	20%	0%	5%	10%	15%	20%
Cucumis sativus	400	1	0.850	0.319	0.319	0.291	0.260	**0.225**	0.186	0.375	0.342	0.306	**0.265**	0.219
		2	0.836	0.290	0.290	0.261	0.229	**0.194**	0.154	0.347	0.313	0.274	**0.232**	0.184
	100	1	0.824	0.316	0.316	0.289	0.260	**0.226**	0.189	0.383	0.351	0.315	**0.275**	0.229
		2	0.823	0.277	0.277	0.248	0.216	**0.181**	0.141	0.339	0.302	0.263	**0.219**	0.171
Spinacia oleracea	400	1	0.781	0.299	0.299	0.274	0.245	**0.214**	0.179	0.379	0.350	0.314	**0.274**	0.229
		2	0.794	0.238	0.238	0.209	0.176	**0.140**	0.099	0.287	0.263	0.222	**0.176**	0.125
	100	1	0.777	0.297	0.297	0.272	0.244	**0.212**	0.177	0.385	0.350	0.314	**0.273**	0.228
		2	0.793	0.244	0.244	0.215	0.183	**0.147**	0.107	0.308	0.271	0.231	**0.186**	0.135
Alocasia odora	100	1	0.851	0.246	0.246	0.214	0.179	**0.139**	0.095	0.286	0.252	0.210	**0.164**	0.111
		2	0.810	0.202	0.202	0.170	0.134	**0.095**	0.050	0.243	0.210	0.166	**0.117**	0.062
	10	1	0.774	0.265	0.265	0.238	0.208	**0.175**	0.138	0.341	0.308	0.269	**0.226**	0.178
		2	0.755	0.224	0.224	0.196	0.165	**0.130**	0.091	0.298	0.260	0.219	**0.173**	0.121
Hordeum vulgare wild type	400	1	0.822	0.274	0.274	0.245	0.213	**0.177**	0.137	0.331	0.298	0.259	**0.216**	0.167
		2	0.797	0.232	0.232	0.202	0.169	**0.132**	0.091	0.294	0.254	0.212	**0.166**	0.114
Hordeum vulgare Chl *b*-less	400	1	0.731	0.238	0.238	0.212	0.183	**0.151**	0.115	0.327	0.290	0.251	**0.207**	0.157
		2	0.694	0.226	0.226	0.201	0.174	**0.143**	0.109	0.333	0.290	0.251	**0.207**	0.157

When FII_m / F_m at 760 nm is γ, and if we assume *RVII* = *RV*690, then equations expressing F_m and *RV* can be written as follows:

$$FI_m760 + \gamma F_m760 = F_m760,$$

and

$$(1-\gamma)\cdot RVI + \gamma \cdot RV690 = RV760.$$

From these, *RVI*, FI_α, FI_β, and the spillover ratio can be obtained as follows:

$$RVI = (RV760 - \gamma \cdot RV690)/(1-\gamma),$$
$$FI_\alpha = (1 - RV760/RV690)/F_m760,$$
$$FI_\beta = (RV760/RV690 - \gamma)/F_m760,$$

and

$$FI_\beta/FI_m = (RV760/RV690 - \gamma)/(1-\gamma).$$

For $FI_\beta > 0$, γ should be $< RV760/RV690$. Note also that FI_α is constant irrespective of γ.

The values for 15% are highlighted in bold as these will be used in the calculations.

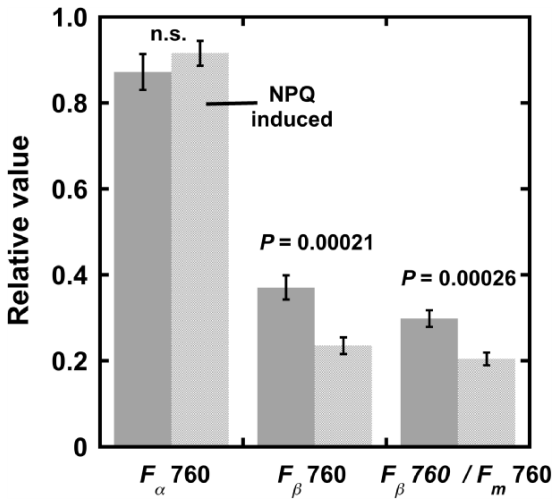

Figure 4. Effects of NPQ induction on spillover of excitations from PSII to PSI in leaf discs from LL *A. odora*. Leaf discs from *A. odora* plants grown at 10 μmol m^{-2} s^{-1} were illuminated with a tungsten lamp at 700 μmol m^{-2} s^{-1} for 270 s, then illuminated with a 720 nm LED at 5 μmol m^{-2} s^{-1} for 10 s to oxidize the plastoquinone pool, and frozen. Inductions of *F*690 and *F*760 were measured. For the control, leaf discs treated in the dark and illuminated with the 720-nm LED at 5 μmol m^{-2} s^{-1} for 10 s were used. *P* values by *t*-test ($n = 4$) are shown. The F_v690/F_m690 values of the dark control and NPQ-induced samples were 0.81 ± 0.014 and 0.77 ± 0.009 ($P = 0.00019$, $n = 4$), while the corresponding F_v760/F_m760 were 0.24 ± 0.012 and 0.15 ± 0.010 ($P = 0.00003$, $n = 4$). Data are all shown as mean ± standard deviation.

was observed in both *A. odora* and *S. oleracea* (Fig. 5a and b). When an unmodulated blue light at 58 μmol m^{-2} s^{-1} was added, the fluorescence level increased to a small extent. This increase was not synchronized with the increase in $P700^+$ (Fig. 5c and d). Moreover, the fluorescence levels did not respond to further increases in the photosynthetic PFD (PPFD) level. Therefore, the increase in the 'PSI' fluorescence on the addition of the blue light would not be related to $P700^+$. Instead, a slight increase in the 'PSI' fluorescence upon the blue light illumination might reflect the PSII fluorescence induction and fluorescence caused by spillover E*s from PSII to PSI. It is probable that the light used for PSI excitation slightly excited PSII. PSII reduction proceeded slowly, because the measuring/actinic beam had a narrow peak at 700 nm and was weak. Judging from the induction shown in Fig. 1, PSII would be fully reduced within 5 s upon illumination of the blue light at 58 μmol m^{-2} s^{-1}. Thus, the PSII fluorescence level excited by the modulated measuring/actinic light would increase. 'PSI' fluorescence caused by the spillover from PSII contributed to this small increase. Once PSII reaction centres were all reduced, further increases in the 'PSI' fluorescence attributable to closure of PSII were not observed even in the stronger actinic lights.

$P700^+$ increased slowly in the weak measuring/actinic light and more rapidly with 58 and 360 μmol m^{-2} s^{-1} blue light (Fig. 5c and d). A further increase in the actinic light to 3000 μmol m^{-2} s^{-1} did not cause a notable increase in $P700^+$, indicating that the $P700^+$ level was nearly saturated. When the 'PSI' traces are compared with those for the $P700^+$, there were no indications of fluorescence changes with the increase in $P700^+$. Upon illumination with 3000 μmol m^{-2} s^{-1} light, some decreases in 'PSI' fluorescence were observed in both spinach and *A. odora*.

Effects of PSII fluorescence on PSI fluorescence

Because the *F*II emission spectrum overlaps with the absorption band of Chl *a*, some *F*II is absorbed by long waveband Chl *a* molecules in PSI. Then, *F*I would be caused not only by the spillover E*s from PSII to PSI but also directly by *F*II. In this section, the leftover of *F*II at 760 nm will not be considered for simplicity.

In our measuring system, the measuring/actinic light was illuminated from one side of the leaf disc and fluorescence emitted from the same side was measured (Supplementary Fig. S1). Chls were excited with the pulse-modulated blue light at 460 nm, and *F*II and *F*I were measured at 690 and 760 nm. Using a simple model, we calculated 460-nm light absorbed by a thin layer, emission of PSII fluorescence by this layer, reabsorption of this fluorescence by the rest of the leaf, and emission of PSI fluorescence due to the reabsorption, in this order. Then, the ratio of the *F*I excited by *F*II to the *F*I directly driven by the 460-nm light was calculated (see Supplementary Text 2 and Supplementary Fig. S6). The calculations indicate that this ratio should increase with the Chl concentration per leaf area or the Chl concentration in the thylakoid suspension (Supplementary Fig. S8). If excitation of PSI by *F*II is substantial, then the 'apparent' *RV*I should increase with the Chl concentration because *RV*II is greater than *RV*I. We examined this possibility by plotting *FV*760 of the suspensions of spinach thylakoids of varying Chl concentrations in a 3-mm thick aluminium cup (see Fig. 6a and Supplementary Fig. S1). We also plotted the *RV*760 against the Chl content in the leaf discs used for Fig. 3 (See Table 1 for Chl contents and Chl *a*/*b* ratios of the samples). We found no dependence of *RV*760 on the chlorophyll content in the sample (Fig. 6a and b). These results indicate that the effect of PSI excitation by *F*II was small in the present measurement. This would be attributed to low PSII fluorescence yield *in vivo*, which is a few percent (Latimer et al. 1956, Lamb et al. 2018).

Chloroplast ultrastructure of *A. odora*

In Fig. 7, electron micrographs of the chloroplasts in the leaves from the *A. odora* plants grown at 180 (HL) and 10 (LL) μmol m^{-2} s^{-1} are shown. These chloroplasts were from the first cell layers in the palisade tissues to avoid the effects of intraleaf light gradient on thylakoid morphologies (Skene 1974, Terashima et al. 1986, Terashima and Hikosaka 1995). Thylakoid membranes per unit volume were more abundant in LL chloroplasts than in HL chloroplasts. Near the chloroplasts, peroxisomes (P) and mitochondria (M) were observed in both samples (Fig. 7a and b). Starch grains (S) and lipid components (plastoglobules) were more conspicuous in HL chloroplasts (Fig. 7a) than in LL chloroplasts (Fig. 7b). In both samples, directions of the

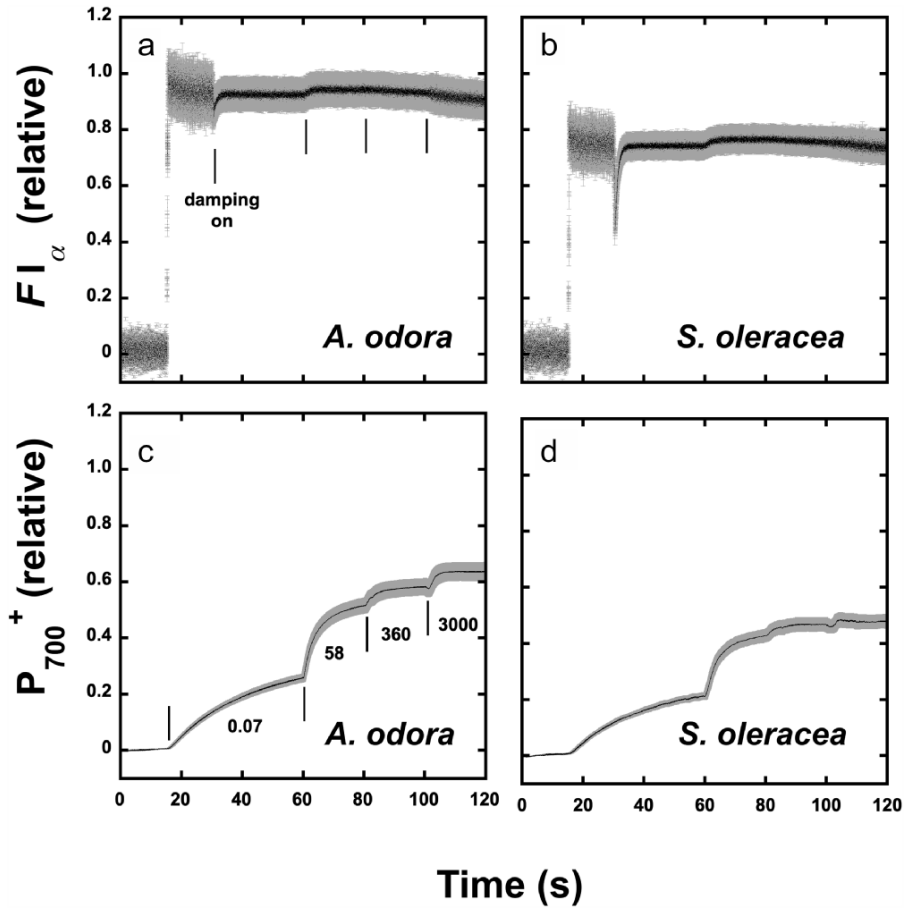

Figure 5. PSI intrinsic fluorescence and $P700^+$ formation. Induction of PSI intrinsic fluorescence excited at 700 nm and measured in the waveband > 730 nm in the leaf discs from*A. odora* grown at 10 μmol m^{-2} s^{-1} (a) and from spinach grown at 400 μmol m^{-2} s^{-1} (b). (c and d) Formation of $P700^+$ in response to 700 nm light at 0.07 μmol m^{-2} s^{-1}, 470 nm blue light at 58 and 360 μmol m^{-2} s^{-1}, and white incandescent light at 3000 μmol m^{-2} s^{-1}. The mean value (blac dot) ± standard deviation (grey bar) are shown ($n = 4$).

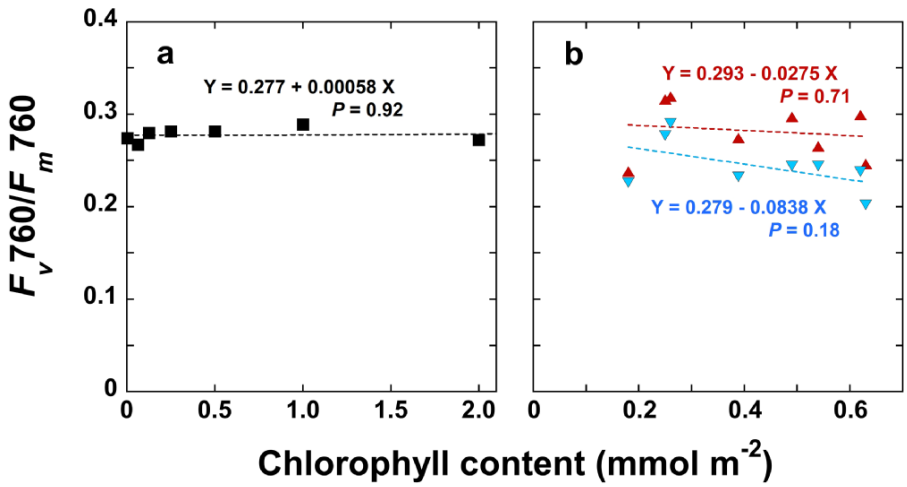

Figure 6. F_v760/F_m760 plotted against the chlorophyll concentration in the spinach thylakoid suspension (a) and in the leaf discs used for Fig. 3(b). (a) Thylakoid suspensions were not preilluminated. The samples were kept in the dark before freezing. (b) Upward-pointing triangles in red denote the data obtained in State 1, while Downward-pointing triangles in blue denote State 2. Equations are the linear regression lines. Neither of the slopes were statistically different from 0.

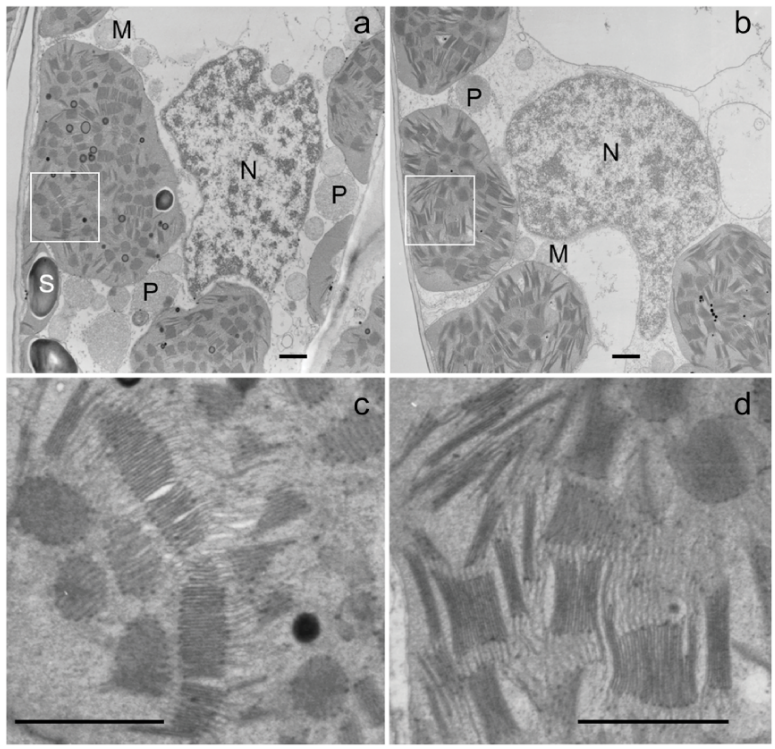

Figure 7. Portions of the palisade tissue cells of *A. odora* leaves grown at high light (a and c) and low light (b and d). For the electron microscopy study, the leaves grown at 180 and 10 μmol m^{-2} s^{-1} were used. Near the well-developed chloroplasts, peroxisomes (P) and mitochondria (M) are observed in both samples (a and b). The square parts in (a) and (b) are enlarged in (c) and (d). Starch grains (S) and lipid components (plastoglobules) are more conspicuous in HL chloroplasts (a) than in LL chloroplasts (b). There are abundant nonappressed thylakoid membranes extending from grana stacks. Bars indicate 1 μm. The nonappressed thylakoid membranes/total thylakoid membranes in the central parts of these chloroplasts were 0.42 and 0.41 (see Figs. S10 and S11).

grana stacks were variable. Thus, both circular face views and side views of grana stacks were seen within the same sections. The diameters of grana were greater in the LL chloroplasts than in HL chloroplasts. The number of thylakoids per granum was somewhat smaller in LL chloroplasts than in HL chloroplasts. In HL chloroplasts, huge grana with numerous thylakoids were occasionally observed. In these huge grana, some thylakoids were swollen, and, in places, stackings were not tight. In both chloroplasts, there were abundant intergranal thylakoids.

In Fig. 8a, the total length of thylakoid membranes per 1 μm^2 of the ultrathin sections is shown. As already described earlier (Fig. 7), thylakoid membranes were more packed in the LL chloroplasts than in HL chloroplasts. The quantitative analysis of the ratios of nonappressed membrane/total thylakoid membranes (Fig. 8b) revealed that the ratios were similar between HL and LL chloroplasts: The intergranal thylakoids were abundant in both HL and LL leaves. For the method used for the measurement of the lengths of nonappressed and appressed membranes, see Supplementary Figs. S10 and S11.

Discussion

Quantitative analyses of the spillover

Recent studies on the spillover have been employing the time-resolved fluorescence spectral analysis (Yokono 2015, Bag et al. 2020). Although time scales of spillover and the roles of respective pigments have been clarified by this method, quantitative analyses of the quantum yield of the spillover may not be feasible. For example, it is hard to estimate how much of E*s move from PSII to PSI, although an attempt to measure the quantum yield of spillover in mixtures of cyanobacterial PSI and PSII preparations based on the steady-state and time-resolved fluorescence spectroscopy has been recently reported (Akhtar et al. 2024). Classically, slower changes in fluorescence at 77 K were analysed (Kitajima and Butler 1975a, b, Kitajima 1976, Strasser and Butler 1977a, b). We followed these classics. We, however, dealt with the *F*II leftover beyond the *F*I peak for the first time, which was neglected in these classical studies.

As shown in Fig. 1, in the time scale of the present study, inductions of PSI and PSII fluorescence were synchronous, as has been shown (Kitajima and Bulter 1975b). Thus, we attributed the main part of PSI induction to the spillover of E*s from PSII. We also assumed that spillover occurs in the absence of closed PSII (Kitajima and Bulter 1975 a, b, Strasser and Butler 1977b). For the diagram of these relationships between *F*I and *F*II, see Supplementary Fig. S3. We assumed that FI_α is constant, which would be supported by the data shown in Figs. 4 and 5. The mathematical equations used for the calculation of FI_α give constant FI_α at any leftover ratios. The constant FI_α values

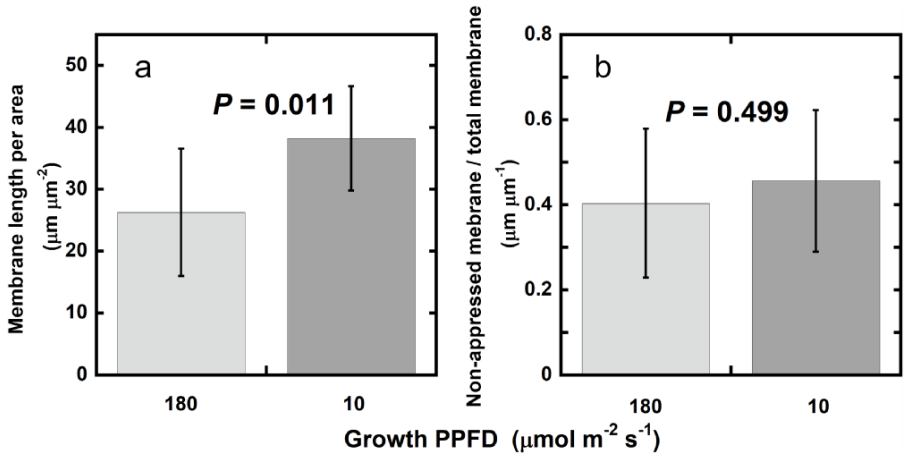

Figure 8. Total length of thylakoid membranes per 1 μm^2 area (a) and the ratio of the cumulative length of nonappressed thylakoid membranes to that of total thylakoid membranes (b). On electron micrographs of chloroplasts, 1 μm^2 in which all the thylakoid membranes were in focus were chosen, and the morphometry data, total thylakoid membrane length (a), and the ratio of the cumulative length of nonappressed thylakoid membranes to that of total thylakoid membranes (b) were obtained for leaf segments from an *A. odora* leaf grown at 180 μmol m^{-2} s^{-1} and that grown at 10 μmol m^{-2} s^{-1}. The bar shows the mean for 10 squares (1 μm^2) from 10 different chloroplasts ± SD.

shown in Figs. 4 and 5, thus, inversely support the relevance of our simple equations in the note for Table 3.

Although these classical studies neglected the *F*II leftover at the long wavelengths, we found the substantial leftover of *F*II at 760 nm. Unfortunately, we could not devise a direct method to quantify the FII_m/F_m. However, we tried to estimate the leftovers from F_m and *RV* (F_v/F_m) spectra, based on the simple assumptions (see Supplementary Text 1). Our estimations of the PSII leftovers range from 10% to 20%. The values in Table 2 may not be regarded as those specific to the species. In particular, the estimation using the quadratic curve for the PSII particles from *A. thaliana* (Ruban and Johnson 2009) would not work properly with the species having different PSII spectral properties. Thus, each of the estimated values should be regarded as an example.

The contribution of spillover to *F*I is summarized in Fig. 3. The lowest value was recorded for the HL *A. odora* treated in State 2 light. However, this was still >0.24. The highest values approached 0.38 in State 1 light. After the correction for the 15% FII_m/F_m at 760 nm, these values were 0.12 and 0.28, respectively (Table 3).

One of the main aims of the present study was to examine whether the spillover occurs in LL chloroplasts. Considerable spillover occurred in the shade-tolerant plant *A. odora*, and the spillover ratio in this plant was greater in the LL leaf than in the HL leaf. In *C. sativus* as well, the LL leaf showed higher spillover ratios, while in *S. oleracea*, the spillover values were similar. Based on the present data, our conclusion is that spillover occurs in both sun and shade chloroplasts.

When NPQ was induced, the spillover from PSII to PSI became smaller. It is also noteworthy that FI_α was unaffected, indicating that NPQ did not develop in the PSI antennae or its effect was negligibly small in PSI. In *Chlamydomonas reinhardtii*, the protonated LHCSR3 is involved in energy dissipation in both PSI and PSII antennae (Tokutsu and Minagawa 2013, Girolomoni et al. 2019). However, its close homologs are not found in land plants.

Using the time-resolved fluorescence spectral analysis, it has been shown that the excited state of deep-trapped Chl *a* is quenched by P700$^+$ in the PSI–PSII megacomplex prepared from *A. thaliana* (Yokono et al. 2019). It is inferred that PSI fluorescence is quenched in the presence of P700$^+$. For the Förster resonance transition of the excitation from excited Pigment A to B to occur, the fluorescence emission spectrum of A should overlap with the absorption spectrum of B. The probability is also proportional to the inverse of the sixth power of the distance between these pigments (Blankenship 2021). Because P700$^+$ has a broad absorption band (Inoue et al. 1973), which overlaps well with the PSI fluorescence emission spectrum from red Chls, Förster resonance transition would be possible from E*s to P700$^+$. When this transition occurs efficiently, quenching of PSI fluorescence with the increase in P700$^+$ may be expected. However, appreciable quenching was not detected in LL *A. odora* or *S. oleracea* (Fig. 5), probably because the quenching was subtle if any, due to the longer distance from the red Chls to P700 (>6 nm) than the distance (∼4.2 nm) in cyanobacteria (Karapetyan et al. 1999, Schlodder et al. 2005).

On the other hand, in the P700-enriched particles (Ikegami 1976) and the PSI preparation (Wientjes and Croce 2012), P700$^+$ increases the PSI fluorescence level. Although Ikegami (1976) found a considerable increase in PSI fluorescence in his PSI particle with the Chl/P700 ratio of 7, he argued that this much increase would be hidden in the thylakoids. Wientjes and Croce (2012) detected a 4% increase in PSI fluorescence with the formation of P700$^+$ in their PSI preparation in which the Chl/P700 ratio would be ∼130. In the data shown in Fig. 5, we were not able to detect the effects of P700

oxidation level on the PSI intrinsic fluorescence level. Thus, at least for the first approximation, we would be able to regard FI_{α} as a constant.

PSI would be excited by PSII fluorescence. The ratio of the PSI fluorescence excited by PSII fluorescence ($FI_{\leftarrow F_{II}}$) to the PSI fluorescence directly excited by the 460 nm light (FI_{direct}) increases with the Chl content per unit area (see Supplementary Text 2 and Supplementary Fig. S7). Then, *RV*760 should also increase with the increase in the Chl content per area. However, this trend was not observed (Fig. 6). $FI_{\leftarrow F_{II}}/FI_{direct}$ may be expressed by Equation S14 (see Supplementary Text 2), which is the product of the yield of PSII fluorescence and the ratio of the integrals. The former would be a few percent (Latimer et al. 1956, Lamb et al. 2018). The latter would be <1–2. Thus, $FI_{\leftarrow F_{II}}/FI_{direct}$ would be a few percent.

Concerning the procedures of the present measurements, it had been better to measure the 'mostly' PSI fluorescence at 750 nm instead at 760 nm. Then, the overestimations of spillover ratios were smaller. The F_v/F_m spectra had to be measured first, and then the wavelength for the mostly PSI fluorescence measurement had to be determined for each of the species. The system used in the present study is not ideal for such measurements. The time-resolved fluorometer that can measure the time-dependent spectral transient from F_0 to F_m such as used in Franck et al. (2002) or Santabarbara et al. (2019) must be ideal. Then, the full spectra can be measured with one leaf disc. We, here, stress that these procedures would be needed for accurate quantification of the spillover.

Spillover in fluorescence quenching analyses

Fluorescence is a useful probe to analyse photosynthetic reactions (Papageorgiou and Govindjee 2004). In many fluorescence models, however, spillover is not considered. Let us assume that the initial allocation of E*s to PSII is Ψ_{II}. Maximum quantum yield of PSII photochemistry on absorbed PFD (Φ_{II}), with no energy-dependent quenching (NPQ), may be expressed as follows (Kono et al. 2024). In the present consideration, we deal with FII_0 and FII_m only.

$$\Phi_{II} = \Psi_{II} \cdot \frac{k_P}{k_P + k_F + k_D + k_{isc} + k_S} = \Psi_{II} \cdot \frac{k_P}{\Sigma k}, \quad (3)$$

where *k*s are the first-order rate constants: k_P, photochemistry; k_F, radiative (fluorescence) de-excitation; k_D, thermal de-excitation to the ground state via pathways other than NPQ; k_{isc}, intersystem crossing leading to the formation of ^{T}Chl*; and *k*s spillover to PSI. Let us assume that the quantum yield of PSII photochemistry *FV*II with fully oxidized PSII in low light is 0.8:

$$FII_v/FII_m = k_P/\sum^k = 0.8. \quad (4)$$

Thus,

$$(k_F + k_D + k_{isc} + k_S)/\sum^k = 1 - k_P/\sum^k = 0.2. \quad (5)$$

In weak light, PSI quantum yield on absorbed PFD basis, Φ_I, is expressed as follows, if one assumes that the quantum yield of PSI photochemistry is 1.0:

$$\Phi_I = 1 - \Psi_{II} + \left(k_S/\sum^k\right) \cdot \Psi_{II}. \quad (6)$$

We may assume that Φ_{II} and Φ_I are identical in weak light for the smooth linear electron transport to occur. Then,

$$\Phi_I = 0.8 \cdot \Psi_{II}. \quad (7)$$

As the spillover ratios in State 1 with closed PSII, after the correction for 15% FII_m/F_m at 760 nm, ranged from 0.16 to 0.28 (Table 3):

$$\frac{FI_{\beta}}{FI_{\alpha} + FI_{\beta}} = \frac{\frac{k_S}{k_F + k_D + k_{isc} + k_S} \cdot \Psi_{II}}{\left(1 - \Psi_{II} + \frac{k_S}{k_F + k_D + k_{isc} + k_S} \cdot \Psi_{II}\right)} = 0.16 - 0.28. \quad (8)$$

Noting $\sum^k = 5 \cdot (k_F + k_D + k_{isc} + k_S)$, we can solve Equations 7 and 8. Then, Ψ_{II} ranges from 0.56 to 0.57 and $k_S/\sum^k$ ranges from 0.029 to 0.058. In other words, even when PSII reaction centres are all open, 2.9–5.8% E*s initially allocated to PSII are redirected to PSI. When all the PSII reaction centres are closed, 15–29% of E*s initially allocated to PSII are transferred to PSI. Although the relative contribution of spillover decreases with the increase in NPQ, the present analyses confirmed that the spillover ratio is large, and it should not be neglected. It is worth pointing out that considering the lower quantum yield of PSII and spillover, the initial allocation of E*s to PSII should be much greater than 0.5, whereas it is usually assumed to be 0.5.

Chloroplast Ultrastructure

Figure 7 shows the chloroplast structure of *A. odora* leaves. As expected, thylakoid membrane length per unit volume was greater in the chloroplasts in the LL leaf than those in the HL leaf. By dividing these lengths by 2, the thylakoid lengths are obtained. Although some swelling was observed in HL thylakoids, assuming a thylakoid thickness of 13 nm (Kirchhoff 2019), volumes of thylakoids per unit chloroplast volume, excluding those of the interthylakoid spaces, were calculated to be 17% and 25% in HL and LL chloroplasts.

For the Förster-type transfer to occur, the set of pigments should be located close enough. For Chls, the distance which allows 50% probability of energy transfer is calculated to be 5–10 nm (Van Grondelle et al. 1994), then the jump across the interthylakoid partition (~4 nm, according to Kirchhoff 2019) would be possible. Then, energy transfer may not be confined to within the same membrane. However, based on analyses of the decay time of fluorescence, it has been argued that the main pathway of the spillover is within the same membrane (Farooq et al. 2016). It is noteworthy that intergrana thylakoids

were extensive and that the fractions of the nonappressed thylakoid membranes were similar and >40% in both HL and LL chloroplasts of *A. odora*. Although the grana morphology has attracted attention (Anderson 1986, Terashima and Hikosaka 1995) and rearrangement of grana in response to light has been shown (Anderson and Andersson 1988, Rozak et al. 2002, Kirchhoff 2019), detailed dynamics of the intergrana thylakoids have not been examined.

The appressed thylakoid membranes may also accommodate megacomplexes in their margins. For example, the size of a PSI–PSII megacomplex of *Oryza sativa* (rice) is ∼25 nm in its major axis (Kim et al. 2023) and the diameter of the granum ranged from 400 to 600 nm (Fig. 7, see also Kirchhoff 2019). Assuming that the grana radius is R (nm) and the megacomplexes are aligned in the margin of the thylakoid with their PSI portions outwards, the area of the thylakoid accommodating the megacomplexes is calculated to be $\left[R^2-(R-25)^2\right]/R^2$. Thus, the marginal area corresponding to 23–16% of the appressed thylakoid membrane may accommodate the megacomplexes. Since the areas of the appressed thylakoids were 60% and 54% of the total areas for HL and LL chloroplasts (Fig. 8), the membrane areas that may accommodate the PSI–PSII megacomplexes would be 53% ($0.40+0.60\times0.23$) and 55% ($0.46+0.54\times0.16$) of the total membrane areas in HL and LL chloroplasts.

Conclusions and a Brief Ecological Consideration

The present study showed that spillover occurs in all plant materials including LL shade-tolerant *A. odora*. The organized spillover would occur within the PSI –PSII megacomplexes in the nonappressed thylakoid membrane and in the marginal areas of appressed thylakoids. It is noteworthy that these parts would comprise >50% of the total thylakoid membrane areas in both HL and LL *A. odora*. In nature, shade-tolerant species are usually in the green shade. In such green shade, FR light is enriched (Kono et al. 2020, 2024). Thus, the thylakoids of these plants are in State 1 and operate photosynthesis at the highest efficiency without NPQ. Upon sudden exposure of such leaves to high light due to sun patches (Smith and Berry 2013) or sunflecks (Pearcy and Way 2012), E*s initially allocated to PSII would be spilt over to PSI most efficiently. Since the decreased electron flow and increased excitation flow to PSI contribute to formation of $P700^+$, the safe quencher, the spillover would protect both PSII and PSI from photoinhibition.

Materials and Methods

Plant Materials

Cucumis sativus L. (cucumber) 'Nanshin', *Spinacia oleracea* L. (spinach) 'Torai', *Alocasia odora* (G. Lodd.) Spach, and *Hordeum vulgare* L. (barley) 'Gunilla, Svalöf AB N83-4001', a wild type, and *H. vulgare* 'Dornaria, chlorina-f2^{2800}', a chlorophyll *b*-less mutant, were grown in vermiculite in pots in growth chambers at 25°C. The light period was 12 h. Light was provided by a bank of white fluorescent lamps. PPFD levels were adjusted with the number of fluorescent tubes and/or the black shade cloth. *C. sativus*, *S. oleracea*, and *A. odora* were grown at two PPFD (400–700 nm) levels. For cucumber and spinach, the PPFD levels were 400 and 100 μmol m^{-2} s^{-1}, while for *A. odora*, 100 and 10 μmol m^{-2} s^{-1} were used. *H. vulgare* plants were grown at 400 μmol m^{-2} s^{-1}. For electron microscopy, *A. odora* grown at 180 and 10 μmol m^{-2} s^{-1} were used. Plants were given the 1/1000 strength of the Hyponex 6–10–5 solution (Hyponex, Japan) diluted with tap water every 2 or 3 days. The relative humidity of the chamber was kept above 50%. The growth light PPFD level of 400 μmol m^{-2} s^{-1} for sun plants or crops would be sufficiently high. At 10 μmol m^{-2} s^{-1}, where *A. odora* showed slow growth, corresponds to PPFD levels on the deep forest floor.

For the assessment of *F*II leftover at 760 nm, we grew *A. odora* and *C. sativus* outdoors in the soil in the pots. The *A. odora* plant used was the clone of the plants used in other measurements. For *C. sativus*, the same variety ('Nanshin') was used. We bought *S. oleracea* from a local market. These measurements were conducted in July 2024, the warmest season.

77 K fluorescence from leaf discs

Fluorescence induction at 77 K was measured using a PAM 101 fluorometer (Walz, Effeltrich, Germany). The original red LED (650 nm) used for the pulse-modulated measuring light was replaced with a blue LED (OSUB5111AST, OptoSupply, Hong Kong) peaked at 460 nm. In the PAM 101 fluorometer, a photodiode was used to detect fluorescence. The original FR filter was replaced with a 690-nm or 760-nm bandpass filter (HMX0690 or HMX0760, Asahi Spectra, Tokyo, Japan) for PSII or mostly PSI fluorescence measurements.

Leaf discs (10 mm in diameter) were cut with a leaf punch. Sixteen leaf discs were used for one series of measurements. For one set of measurements, four leaf discs were used and fluorescence inductions were measured at 690 and 760 nm, respectively, in States 1 and 2. These four discs were taken from a narrow uniform part of a leaf. For *C. sativus*, *S. oleracea*, and *A. odora*, 16 leaf discs were taken from one leaf, whereas for *H. vulgare*, four sets were taken from four separate leaves. The leaf discs were placed on wet filter paper with the adaxial sides upward and illuminated with State 2 light at 470 nm from LEDs (L470, Ushio, Tokyo) or State 1 light at 720 nm from LEDs (L720, Ushio, Tokyo) at a PFD of 10 μmol m^{-2} s^{-1} at a room temperature of ca. 25°C. For *A. odora* leaves grown at 10 μmol m^{-2} s^{-1}, the PFD level was lowered to 5 μmol m^{-2} s^{-1}. After illumination for at least 30 min with either of the State 1 or State 2 LEDs, the adaxial side of leaf disc was attached to a quartz rod with silicone grease and covered with an aluminium cap and dipped in liquid nitrogen in a Dewer jar. From the cessation of the State light treatment until freezing, all the procedures were performed within 1.5–2 min in dim light. After the enclosure in the cup, the sample was further darkened. When the temperature of the sample in the aluminium cap was equilibrated with that of liquid nitrogen, which was detectable by a change in the sound of bubbling, recording was started. After 2 s, the measuring/actinic blue light at 50 μmol m^{-2} s^{-1} (pulse modulated at 100 kHz) was turned on. The fluorescence induction at 690 or 760 nm was recorded at 1-ms time intervals for 28 s on a USB data acquisition system (USB-1608FS, Measurement Computing, Norton, MA, USA). For the measurement system, see Supplementary Fig. S1. For transmittance spectra of 690 and 760 nm bandpass filters, see Supplementary Fig. S2.

The F_v/F_m (*RV*) spectra in the wavelength range from 690 to 780 nm were obtained as described earlier. Emission spectra of F_m, excited by blue light from an LED peaked at 450 nm, were measured using a photodiode array spectrophotometer (C10083CAH, Hamamatsu Photonics, Japan) and an optical system similar to that used for the *RV* measurement. For details, see Terashima et al. (2021) and Supplementary Fig. S1. *RV* in the leaf discs was measured as described earlier using the band pass filters (Asahi Spectra). The leaf discs were treated in State 1 light at 720 nm at 10 μmol m^{-2} s^{-1} at least for 30 min.

Effects of NPQ on the spillover

The effects of NPQ on the spillover were examined using an *A. odora* leaf grown at 10 μmol m^{-2} s^{-1} light. The leaf disc attached to a quartz rod was covered

with an aluminium cap, and NPQ was induced by illuminating the leaf disc with an actinic white light from a tungsten lamp (KL1500 LSCD, Schott, Mainz, Germany) at 700 μmol m^{-2} s^{-1} for 270 s at a room temperature of ca. 23°C. Saturating flashes at 6600 μmol m^{-2} s^{-1} for 1 s were given at 20-s intervals. The actinic light was turned off, and 10 s after, the measuring beam was turned off. At 5 s after turning off the actinic light, FR light peaked at 720 nm at 10 μmol m^{-2} s^{-1} was illuminated for 10 s to oxidize PSII. Then, the leaf disc in the cap was frozen at 77 K. When the temperature reached 77 K, PSI or PSII fluorescence was measured as earlier.

Effects of P700+ formation on PSI fluorescence

PSI fluorescence was obtained by preferential illumination of PSI pigments. The actinic/measuring light was a 700-nm LED (5 mm bullet type, Ushio, Tokyo, Japan) passing through a 700-nm band pass filter with a 10-nm half-band width (HMX700, Asahi Spectra, Tokyo, Japan) and a 710-nm short pass filter (SVX 710). For detection of PSI fluorescence, the photodiode of the PAM 101 covered with a long pass filter (LVX 730, allowing transmission of FR light > 730 nm) was used. Since it was necessary to use the measuring/actinic light of the very narrow waveband, the PFD level at the leaf disc surface was 0.07 μmol m^{-2} s^{-1}.

The leaf disc kept in the dark at least for 30 min was attached to the quartz rod, enclosed by an aluminium cup, chilled at 77 K, and its PSI fluorescence was measured. The accumulation of $P700^+$ was measured with a dual-wavelength (820/870 nm) unit (ED-P700DW) attached to a PAM fluorometer (Walz) in the reflectance mode. When the two PAM101 systems were operated at the same time, the signals sometimes became noisy. Thus, we used similar leaf discs taken from the same leaf and measured the PSI fluorescence and redox state of P700 separately, but according to the same illumination time schedule.

After the onset of recording at 4-ms intervals, the measuring/actinic light for PSI at 0.07 μmol m^{-2} s^{-1} was on at 15 s. The noise reduction circuit was turned on to reduce the noise level at 30 s, an unmodulated blue light at 58 μmol m^{-2} s^{-1} from 460 nm LED was added at 60 s, the blue light level was increased to 360 μmol m^{-2} s^{-1} at 80 s, and, the blue light was turned off, a white light from a tungsten lamp at 3000 μmol m^{-2} s^{-1} was turned on at 100 s. When the redox state of P700 was measured, the pulse-modulated measuring light from a PAM 101 FR LED emitting light with wavelengths ranging from 800 to 900 nm was used.

Effects of excitation of PSI fluorescence by reabsorbed PSII fluorescence

To examine the effects of Chl concentration on PSI fluorescence excited by reabsorbed PSII fluorescence, thylakoids were prepared from the laboratory-grown spinach at 400 μmol m^{-2} s^{-1} PPFD (see earlier) as described in Terashima et al. (2021). PSI fluorescence induction in the thylakoid suspension in a buffer containing 0.3 M sorbitol, 10 mM NaCl, 5 mM $MgCl_2$, and 50 mM and Hepes-KOH (pH at 8.0) was measured at 77 K in a 3-mm thick aluminium cuvette (see Supplementary Fig. S1). All these procedures were performed in dim light. The pulse-modulated measuring/excitation light at 460 nm used was at the PPFD of 12 μmol m^{-2} s^{-1}. The weaker light was used to obtain more data points for the induction phase with the diluted thylakoid suspensions. For theoretical consideration, see Supplementary Text 2.

Data processing

F_0 and F_m determination for leaf discs. The recording system was turned on at 0 s, and the measuring/actinic light was turned on at 2 s. The zero (0) and the maximum fluorescence (F_m) levels were obtained by averaging 2000 data points between 0 and 2 s and between 28 and 30 s. A linear regression equation was obtained using the 50 data points, from 2.005 to 2.054 s. F_0 was obtained by substituting 2 s to this equation.

F_m and F_0 thus obtained were used to calculate F_v ($= F_m - F_0$) and F_v/F_m. As the increases in PSI and PSII fluorescence intensities were synchronous (Fig. 1), the variable fluorescence in PSI was assumed to be attributed to the spillover from PSII variable fluorescence.

The spillover from PSII to PSI was assumed to occur at the same efficiency regardless of whether PSII reaction centres were open or closed (Strasser and Butler 1977a, b). Based on these assumptions, and assuming that PSII and PSI fluorescence could be separately measured at 690 and 760 nm, PSI fluorescence at time t, $F\mathrm{I}(t)$, was expressed as follows:

$$F\mathrm{I}(t) = F\mathrm{I}_\alpha + \sigma \cdot F\mathrm{II}(t), \tag{9}$$

where σ is the spillover coefficient. From this, intrinsic PSI fluorescence ($F\mathrm{I}_\alpha$) was obtained:

$$F\mathrm{I}_\alpha = F\mathrm{I}_m - F\mathrm{I}_v/(F\mathrm{II}_v/F\mathrm{II}_m). \tag{10}$$

Induction time determination. Assuming that the PSII fluorescence induction occurred in two phases, the induction curve was fitted by the equation:

$$F(t) = F_0 + \cdot a \cdot [1 - \exp(-k_1 \cdot t)] + (F_m - F_0 - a) \cdot [1 - \exp(-k_2 \cdot t)]. \tag{11}$$

We used F_0 and F_m, which were obtained as earlier. Constants, a, k_1, and k_2 were obtained by the fitting with KaleidaGraph (Version 5.0, Synergy Software). Then, $t_{1/2}$ was obtained as t giving $F(t) = F_0 + (F_m - F_0)/2$.

F_0 determination for thylakoid suspension. Since a weaker actinic/measuring light was used for thylakoid suspensions, the linear regression of 50 data points was not reliable due to the lower S/N ratio. When the number of data points was simply increased, linearity could not be assumed. Thus, we fitted Equation 8 to the fluorescence transient for 2 s to obtain F_0, a, k_1, and k_2. Because time constant k_2 was always one order of magnitude smaller than k_1, we further assumed that $k_2 = 0.1 \cdot k_1$. The determination coefficients obtained with this assumption were always greater than those for the equation in which k_1 and k_2 were independently obtained.

Electron microscopy

The *A. odora* plants used were grown at the PPFD 180 or 10 μmol m^{-2} s^{-1}. After harvesting, the leaves were kept in the dark at room temperature for at least 30 min before fixation. Leaf segments, ca. 1 mm × 4 mm were excised and fixed immediately in 2% glutaraldehyde in 0.05 M potassium phosphate buffer (pH 6.8) and kept at room temperature for 2 h and then at 4°C overnight. Six rinses in the buffer solution preceded postfixation with 2% OsO_4 in the buffer at room temperature for 2 h. After dehydration in a graded acetone series, leaf materials were embedded in Spurr's resin. The ultrathin sections (silver-gold) were poststained with uranyl acetate and lead citrate and examined with a Hitachi H-7500 transmission electron microscope at an accelerating voltage of 80 kV.

Electron micrographs of the first cell layers of the palisade tissues were taken to avoid the effects of intraleaf light gradient on thylakoid morphologies (Skene 1974, Terashima et al. 1986, Terashima and Hikosaka 1995). In the leaves grown at 180 or 10 μmol m^{-2} s^{-1} light, 36 or 30 chloroplasts were randomly chosen, and in these chloroplasts, 178 or 157 squares of 1 μm^2, in which all thylakoid membranes were in focus, were selected randomly. We randomly selected 10 of these squares from 10 chloroplasts for each growth light level and thylakoid lengths were measured using Fiji/ImageJ (National Institutes of Health).

The total length of the thylakoid membranes per 1 μm^2 was also calculated as an index of thylakoids to stroma volume ratio. The abundance of nonappressed thylakoids was expressed as the ratio of the length of the nonappressed thylakoid membranes to the total thylakoid membranes. For examples of tracing the electron micrographs, see Supplementary Figs. S10 and S11.

Symbols and abbreviations

Chl, chlorophyll; Chl*, exited state of chlorophyll; E*, chlorophyll excitation; F, fluorescence; F_0, minimum fluorescence; $F690$, fluorescence measured at 690 nm; $F760$, fluorescence measured at 760 nm; I, PSI fluorescence; $F\mathrm{I}_\alpha$, intrinsic

PSI fluorescence; FI_{β}, PSI fluorescence caused by spillover; *F*II, PSII fluorescence; $F\lambda$, fluorescence measured at λ nm; F_m, maximum fluorescence; F_v, variable fluorescence; PFD, photon flux density; PPFD, photosynthetic photon flux density; *RV*, variable fluorescence ratio ($= F_v/F_m$).

Acknowledgments

The barley seeds were a kind gift of Professor W.S. Chow. We thank Professor W. S. Chow, Dr D. Y. Fan, Dr E. Kim, Dr M. Kitajima, Dr M. Yokono for constructive comments. We also thank Dr G. Schansker for drawing our attention to PSI fluorescence excited by PSII fluorescence. We are grateful to Mr H. Hashimoto and Mr A. Okamoto, Namoto Co., Ltd., for assisting modification of the PAM 101. We thank Professor Alexander Ruban for providing a fluorescence spectrum of the BBY PSII from *A. thaliana*. We examined the leftover PSII fluorescence at 760 nm in response to the comments by reviewers I and II. We thank them for their fundamental comments.

Author contributions

All the authors contributed to this study and are responsible for the content of this paper.

Supplementary data

Supplementary data is available at *PCP* online.

Conflict of interest

None declared.

Funding

This work was partly supported by grants from Japan Society for the Promotion of Science (17H05718, 19H04718, 22H02640, and 23K23903) and a Yushan Fellow Scholarship to I.T. from the Ministry of Education, Taiwan.

Data availability

The authors confirm that the data supporting the findings of this study are available within the article and its Supplementary data. Further details of this study are available from the corresponding author (I.T.) upon request.

References

Akhtar, P., Balog-Vig, F., Han, W., Li, X., Han, G., Shen, J.-R., et al. (2024) Quantifying the energy spillover between photosystem II and I in cyanobacterial thylakoid membranes and cells. *Plant Cell Physiol*. 65: 95–106.

Anderson, J.M. (1986) Photoregulation of the composition, function, and structure of thylakoid membranes. *Annu. Rev. Plant Physiol*. 37: 93–136.

Anderson, J.M. and Andersson, B. (1988) The dynamic photosynthetic membrane and regulation of solar energy conversion. *Trend. Biochem. Sci*. 13: 351–355.

Bag, P., Chukhutsina, V., Zhang, Z., Paul, S., Ivanov, A.G., Shutova1, T., et al. (2020) Direct energy transfer from photosystem II tophotosystem I confers winter sustainability in Scots Pine. *Nat. Comm*. 11: 6388.

Bassi, R. and Dall'Osto, L. (2021) Dissipation of light energy absorbed in excess: the molecular mechanisms. *Annu. Rev. Plant Biol*. 72: 47–76.

Bellaflore, S., Barneche, F., Peltler, G. and Rochaix, J.D. (2005) State transitions and light adaptation require chloroplast thylakoid protein kinase STN7. *Nature* 433: 892–895.

Björkman, O. (1981) Responses to different quantum flux densities. *In* Encyclopedia of Plant Physiology, New Series, Vol. 12A. Edited by Lange, O.K., Nobel, P.S., Osmond, C.B. and Ziegler, H. pp. 57–106. Springer, Berlin.

Blankenship, R.E. (2021) Molecular Mechanisms of Photosynthesis. 3rd edn. p. 328. Wiley, Hoboken.

Chow, W.S., Qian, L., Goodchild, D.J. and Anderson, J.M. (1988) Photosynthetic acclimation of *Alocasia macrorrhiza* (L.) G. Don. *Aust. J. Plant Physiol*. 15: 107–122.

Chukhutsina, V.U., Holzwarth, A.R. and Croce, R. (2019) Time-resolved fluorescence measurements on leaves: principles and recent developments. *Photsynth. Res*. 140: 3555–3369.

Demmig-Adams, B. and Adams III, W.W. (2006) Photoprotection in an ecological context: the remarkable complexity of thermal energy dissipation. *New Phytologist* 172: 11–21.

Farooq, S., Chmeliov, J., Trinkunas, G., Valkunas, L. and van Amerongen, H. (2016) Is there excitation energy transfer between different layers of stacked photosystem-II-containing thylakoid membranes?. *J. Phys. Chem. Lett*. 7: 1406–1410.

Franck, F., Juneau, P. and Popovic, R. (2002) Resolution of the Photosystem I and Photosystem II contributions to chlorophyll fluorescence of intact leaves at room temperature. *Biochim. Biophys. Acta* 1556: 239–246.

Garcia-Molina, A. and Leister, D. (2020) Accelerated relaxation of photoprotection impairs biomass accumulation in *Arabidopsis*. *Nat Plant* 6: 9–12.

Girolomonia, L., Cazzanigaa, S., Pinnola, A., Perozenia, F., Ballottaria, M. and Bassi, R. (2019) LHCSR3 is a nonphotochemical quencher of both photosystems in *Chlamydomonas reinhardtii*. *Proc. Natl. Acad. Sci. U.S.A*. 116: 4212–4217.

Grieco, M., Tikkanen, M., Paakkarinen, V., Kangasjärvi, S. and Aro, E.M. (2012) Steady-state phosphorylation of light-harvesting complex II proteins preserves photosystem I under fluctuating white light. *Plant Physiol*. 160: 1896–1910.

Horton, P. and Lee, P. (1985) Phosphorylation of chloroplast membrane proteins partially protects against photoinhibition. *Planta* 165: 37–42.

Ifuku, K. (2023) Diversity of the PSI–PSII megacomplexes that conduct energy spillover in green plants. *Plant Cell Physiol*. 64: 844–846.

Ikegami, I. (1976) Fluorescence changes related in the primary photochemical reaction in the P-700-enriched particles isolated from spinach chloroplasts. *Biochim. Biophys. Acta* 449: 245–258.

Inoue, Y., Ogawa, T. and Shibata, K. (1973) Light-induced spectral changes of P700 in the 800-nm region in *Anacystis* and spinach lamellae. *Biochim. Biophys. Acta* 305: 483–487.

Karapetyan, N.V., Holzwarth, A. and Rögner, M. (1999) The photosystem I trimer of cyanobacteria: molecular organization excitation dynamics and physiological significance. *FEBS Lett*. 460: 395–400.

Karlický, V., Podolinská, J., Nadkanská, L., Štroch, M. and Čajánek, M. and Špunda, V. (2010) Pigment composition and functional state of the thylakoid membranes during preparation of samples for pigment-protein complexes separation by nondenaturing gel electrophoresis. *Photosynthetica* 48: 475–480.

Kasahara, M., Kagawa, T., Oikawa, K., Suetsugu, N., Miyao, M. and Wada, M. (2002) Chloroplast avoidance movement reduces photodamage in plants. *Nature* 420: 829–832.

Khorobrykh, S., Havurinne, V., Mattila, H. and Tyystjärvi, E. (2020) Oxygen and ROS in photosynthesis. *Plants* 9: 91.

Kim, E., Yokono, M., Tsugane, T., Ishii, A., Noda, C. and Minagawa, J. (2023) Formation of a stable PSI–PSII megacomplex in rice that conducts energy spillover. *Plant Cell Physiol*. 64: 858–865.

Kirchhoff, H. (2019) Chloroplast ultrastructure in plants. *New Phytologist* 223: 565–574.

Kitajima, M. (1976) Light-induced redistribution of excitation energy in leaves as observed in terms of fluorescence induction. *Plant Cell Physiol*. 17: 921–930.

Kitajima, M. and Butler, W.L. (1975a) Quenching of chlorophyll fluorescence and primary photochemistry in chloroplasts by dibromothymoquinone. *Biochim. Biophys. Acta* 376: 105–115.

Kitajima, M. and Butler, W.L. (1975b) Excitation spectra for photosystem I and photosystem II in chloroplasts and the spectral characteristics of the distribution of quanta between the two photosystems. *Biochim. Biophys. Acta* 408: 297–305.

Kono, M., Kawaguchi, H., Mizusawa, N., Yamori, W., Suzuki, Y. and Terashima, I. (2020) Far-red light accelerates photosynthesis in the low-light phases of fluctuating light. *Plant Cell Physiol*. 61: 192–202.

Kono, M., Oguchi, R. and Terashima, I. (2024) Photoinhibition of PSI and PSII in nature and in the laboratory: ecological approaches. *Progr. Bot*. 84: 241–292.

Kromdijk, J., Głowacka, K., Leonelli, L., Gabilly, S.T., Iwai, M., Niyogi, K.K., et al. (2016) Improving photosynthesis and crop productivity by accelerating recovery from photoprotection. *Science* 354: 857–861.

Lamb, J.J., Røkke, G. and Hohmann-Marriot, M.F. (2018) Chlorophyll fluorescence emission spectroscopy of oxygenic organisms at 77 K. *Photosynthetica* 56: 105–124.

Latimer, P., Bannister, T.T. and Rabinowitch, E. (1956) Quantum yields of fluorescence of plant pigments. *Science* 124: 585–586.

Miyake, C. (2020) Molecular mechanisms of oxidation of P700 and suppression of ROS production in photosystem I in response to electron-sink limitations in C3 plants. *Antioxidants* 9: 230.

Murata, N. (1969) Control of excitation transfer in photosynthesis. I. Light-induced change of chlorophyll a fluorescence in *Porphyridium cruentum*. *Biochim. Biophys. Acta* 172: 242–251.

Papageorgiou, G.C. and Govindjee, G. (2004) Chlorophyll *a* Fluorescence. A Signature of Photosynthesis. p. 818. Springer, Dordrecht.

Pastenes, C., Pimentel, P. and Lillo, J. (2005) Leaf movements and photoinhibition in relation to water stress in field-grown beans. *J. Exp. Bot*. 56: 425–433.

Pearcy, R.W. (1990) Sunflecks and photosynthesis in plant canopies. *Ann. Rev. Plant Physiol. Plant Mol. Biol*. 41: 421–453.

Pursiheimo, S., Rintamäki, E., Baena-Gonzalez, E. and Aro, E.M. (1998) Thylakoid protein phosphorylation in evolutionally divergent speciesswith oxygenic photosynthesis. *FEBS Lett*. 423: 178–182.

Rintamäki, E., Salonen, M., Suoranta, U.-M., Carlberg, I., Andersson, B. and Aro, E.M. (1997) Phosphorylation of light-harvesting complex II and photosystem II core proteins shows different irradiance-dependent regulation in vivo. *J. Biol. Chem*. 272: 30476–30482.

Rozak, P.R., Seiser, R.M., Wacholtz, W.F. and Wise, R.R. (2002) Rapid, reversible alterations in spinach thylakoid appression upon changes in light intensity. *Plant Cell Environ*. 25: 421–429.

Ruban, A.V. and Johnson, M.P. (2009) Dynamics of higher plant photosystem cross-section associated with state transitions. *Photosynth Res*. 99: 173–183.

Ruban, A.V., Johnson, M.P. and Duffy, C.D.P. (2012) The photoprotective molecular switch in the photosystem II antenna. *Biochim. Biophys. Acta* 1817: 167–181.

Santabarbara, S., Villafiorita Monteleone, F., Remelli, W., Rizzo, R., Menin, B. and Casazza, A.P. (2019) Comparative excitation-emission dependence of the F_V/F_M ratio in model green algae and cyanobacterial strains. *Physiol. Plant*. 166: 351–364.

Schlodder, E., Çetin, M., Byrdin, M., Terekhovac, I.V. and Karapetyan, N.V. (2005) $P700^{+}$- and $^{3}P700$-induced quenching of the fluorescence at 760 nm in trimeric Photosystem I complexes from the cyanobacterium *Arthrospira platensis*. *Biochim. Biophys. Acta* 1706: 53–67.

Skene, D.S. (1974) Chloroplast structure in mature apple leaves grown under different levels of illumination and their response to changed illumination. *Proc. R. Soc. London B* 186: 75–78.

Smith, W.K. and Berry, Z.C. (2013) Sunflecks?. *Tree Physiol*. 33: 233–237.

Strasser, R. and Butler, W.L. (1977a) Energy transfer and the distribution of excitation energy in the photosynthetic apparatus of spinach chloroplasts. *Biochim. Biophys. Acta* 460: 230–238.

Strasser, R. and Butler, W.L. (1977b) The yield of energy transfer and the spectral distribution of excitation energy in the photochemical apparatus of flashed bean leaves. *Biochim. Biophys. Acta* 462: 295–306.

Terashima, I. and Hikosaka, K. (1995) Comparative ecophysiology of leaf and canopy photosynthesis. *Plant Cell Environ*. 18: 1111–1128.

Terashima, I., Matsuo, M., Suzuki, Y., Yamori, W. and Kono, M. (2021) Photosystem I in low light-grown leaves of *Alocasia odora*, a shade-tolerant plant, is resistant to fluctuating light-induced photoinhibition. *Photosynth Res*. 149: 69–82.

Terashima, I., Sakaguchi, S. and Hara, N. (1986) Intra-leaf and intercellular gradients in chloroplast ultrastructure of dorsiventral leaves illuminated from the adaxial or abaxial side during their development. *Plant Cell Physiol* 27: 1023–1031.

Tokutsu, R. and Minagawa, J. (2013) Energy-dissipative supercomplex of photosystem II associated with LHCSR3 in *Chlamydomonas reinhardtii*. *Proc. Natl. Acad. Sci. U.S.A*. 110: 10016–10021.

Trrisl, H.-W., Breton, J., Deprez, J. and Leibl, W. (1987) Primary electrogenic reactions of photosystem II as probed by the light-gradient method. *Biochim. Biophys. Acta* 893: 305–319.

Van Dorssen, R.J., Plijter, J.J., Dekker, J.P., Den Ouden, A., Amesz, J. and Van Gorkom, H.J. (1987) Spectroscopic properties of chloroplast grana membranes and of the core of photosystem II. *Biochim. Biophys. Acta* 890: 1324–143.

Van Grondelle, T., Dekker, J.P., Gillbro, T. and Sundstrom, V. (1994) Energy transfer and trapping in photosynthesis. *Biochim. Biophys. Acta* 1187: 1–65.

Weis, E. (1985) Light-and temperature-induced changes in the distribution of excitation energy between Photosystem I and Photosystem II in spinach leaves. *Biochim. Biophys. Acta* 807: 118–126.

Wientjes, E. and Croce, R. (2012) PMS: photosystem I electron donor or fluorescence quencher. *Photosynth Res*. 111: 185–191.

Yokono, M., Takabayashi, A., Akimoto, S. and Tanaka, A. (2015) A megacomplex composed of both photosystem reaction centers in higher plants. *Nat. Comm*. 6: 6675.

Yokono, M., Takabayashi, A., Kishimoto, J., Fujita, T., Iwai, M., Murakami, A., et al. (2019) The PSI–PSII megacomplex in green plants. *Plant Cell Physiol*. 60: 1098–1108.